Title
Experimental realization of linearly polarized x-ray detected ferromagnetic resonance

Journal
New Journal of Physics, 24(1)

ISSN
1367-2630

Authors
Klewe, C
Emori, S
Li, Q
et al.

Publication Date
2022

DOI
10.1088/1367-2630/ac465f

Peer reviewed

PAPER • OPEN ACCESS

Experimental realization of linearly polarized x-ray detected ferromagnetic resonance

To cite this article: C Klewe *et al* 2022 *New J. Phys.* **24** 013030

New Journal of Physics
The open access journal at the forefront of physics

Deutsche Physikalische Gesellschaft DPG
IOP Institute of Physics

Published in partnership with: Deutsche Physikalische Gesellschaft and the Institute of Physics

OPEN ACCESS

RECEIVED
20 July 2021

REVISED
17 December 2021

ACCEPTED FOR PUBLICATION
24 December 2021

PUBLISHED
19 January 2022

PAPER

Experimental realization of linearly polarized x-ray detected ferromagnetic resonance

C Klewe[1,*], S Emori[2], Q Li[3], M Yang[4], B A Gray[5], H-M Jeon[6], B M Howe[5], Y Suzuki[7,8], Z Q Qiu[9], P Shafer[1,*] and E Arenholz[1]

[1] Advanced Light Source, Lawrence Berkeley National Laboratory, Berkeley, CA, United States of America
[2] Department of Physics, Virginia Tech, Blacksburg, VA, United States of America
[3] National Synchrotron Radiation Laboratory, University of Science and Technology of China, Hefei, Anhui, People's Republic of China
[4] Institute of Physical Science and Information Technology, Anhui University, Hefei, Anhui, People's Republic of China
[5] Materials and Manufacturing Directorate, Air Force Research Laboratory, Wright-Patterson Air Force Base, OH, United States of America
[6] Sensors Directorate, Air Force Research Laboratory, Wright-Patterson Air Force Base, OH, United States of America
[7] Geballe Laboratory for Advanced Materials, Stanford University, Stanford, CA, United States of America
[8] Department of Applied Physics, Stanford University, Stanford, CA, United States of America
[9] Department of Physics, University of California at Berkeley, Berkeley, CA, United States of America
[*] Author to whom any correspondence should be addressed.

E-mail: cklewe@lbl.gov and pshafer@lbl.gov

Keywords: XMCD, XMLD, XFMR, antiferromagnetic, FMR, dynamic XMLD

Supplementary material for this article is available online

Abstract

We present the first theoretical and experimental evidence of time-resolved dynamic x-ray magnetic linear dichroism (XMLD) measurements of GHz magnetic precessions driven by ferromagnetic resonance in both metallic and insulating thin films. Our findings show a dynamic XMLD in both ferromagnetic $Ni_{80}Fe_{20}$ and ferrimagnetic $Ni_{0.65}Zn_{0.35}Al_{0.8}Fe_{1.2}O_4$ for different measurement geometries and linear polarizations. A detailed analysis of the observed signals reveals the importance of separating different harmonic components in the dynamic signal in order to identify the XMLD response without the influence of competing contributions. In particular, RF magnetic resonance elicits a large dynamic XMLD response at the fundamental frequency under experimental geometries with oblique x-ray polarization. The geometric range and experimental sensitivity can be improved by isolating the 2ω Fourier component of the dynamic response. These results illustrate the potential of dynamic XMLD and represent a milestone accomplishment toward the study of GHz spin dynamics in systems beyond ferromagnetic order.

To date, antiferromagnetic spintronics represents one of the most active fields in condensed matter research. In particular, ferromagnet (FM)/antiferromagnet (AFM) heterostructures offer great potential for implementation in ultrafast, high-performance solid-state devices, as they can exhibit intriguing effects, e.g., spin orbit torque induced magnetization switching in the absence of external fields [1, 2], and enhanced spin transport across interfaces, despite large frequency mismatch between ferromagnetic (GHz) and antiferromagnetic (THz) resonances [3–8]. Yet, to date the mechanisms responsible for this GHz spin current propagation in AFMs are not well understood. Furthermore, recent studies have shown spin current generation in antiferromagnetic materials well below the THz regime by detecting the DC components of the spin excitation indirectly via spin Hall voltage [9, 10]. To gain deeper insights and enable a fuller understanding of the mechanisms driving these effects, it would be invaluable to perform time-resolved measurements with sensitivity to individual magnetic elements, ions, or sublattices for studying GHz driven magnetization dynamics in systems with antiferromagnetic order. However, experimental techniques that

offer these capabilities are lacking. X-ray detected ferromagnetic resonance (XFMR) with circularly polarized x-rays, i.e., dynamic x-ray magnetic circular dichroism (XMCD) [11–13], has proven an indispensable tool in the investigations of spin dynamics in magnetic multilayers [7, 8, 14–26]. By combining the capabilities of ferromagnetic resonance (FMR) and x-ray absorption spectroscopy as the underlying characterization mechanism, dynamic XMCD can probe magnetic precessions with element specificity, valence state sensitivity, and phase resolution. XFMR has enabled the determination of effective spin mixing conductance of a spin valve with multiple spin sink layers [26], resolving interlayer anisotropic Gilbert damping effects in magnetic source and sink layers coupled by spin pumping [24], and the detection of coherent AC spin current propagation through antiferromagnetic CoO [7] and NiO [8]. Analogous to its static counterpart, dynamic XMCD is sensitive to ferromagnetic order and probes the net vector sum of magnetic moments associated with a certain element or ion.

X-ray magnetic linear dichroism (XMLD) on the other hand can provide information about long range magnetic order even in the absence of a net magnetization and is therefore well suited to study antiferromagnetic materials [27–29]. Interactions between linearly polarized x-rays and magnetic materials under the condition of FMR should produce a dynamic XMLD response from the non-equilibrium evolution of ferromagnetic or antiferromagnetic order.

In this letter, we aim to characterize these interactions in two model systems, a ferromagnetic metal, i.e., $Ni_{80}Fe_{20}$ (Py), and a ferrimagnetic insulator, i.e., $Ni_{0.65}Zn_{0.35}Al_{0.8}Fe_{1.2}O_4$ (NZAFO) [39], whose atomic moments can be readily probed by XMCD or XMLD, thereby enabling a direct comparison of these responses. Both of these systems exhibit low damping, as well as pronounced magnetic circular and linear dichroism signals that aid in the interpretation of the experimental results. We discuss our findings within a theoretical framework and analyze the different contributions to the observed signal for different experimental geometries. Our results represent the first experimental realization of time-resolved dynamic XMLD and constitute a substantial development in the study of GHz spin dynamics. While the time resolution of our setup is ideally suited for investigations in the GHz frequency domain, this new technique can readily be envisioned as a potential pathway to the direct observation of antiferromagnetic THz dynamics when combined with ultrafast x-ray sources (e.g., x-ray free electron laser (XFEL) facilities or gyrotron sources) in future studies.

It should be noted that Boero *et al* previously reported XFMR using linearly polarized x-rays in a time-averaged geometry [33]. While time-averaged XFMR experiments can probe the DC component of a spin excitation, time-resolved measurements are sensitive to the AC component and the phase of the spin precession. This is imperative when studying coherent AC spin current effects.

Previously we utilized dynamic XMLD to evaluate the origin of AC spin current propagation in antiferromagnetic CoO [7]. Due to the absence of CoO evanescent modes in this system we did not detect a dynamic XMLD signal. In contrast, here we present the first conclusive demonstration of a finite phase-resolved dynamic XMLD signal in a ferro- and a ferrimagnetic material and provide a comprehensive model to understand the observed contributions to the dynamic response.

We begin by considering the geometric dependence of dynamic XMLD, which is expected to differ from that of dynamic XMCD in XFMR experiments. This is primarily because XMCD is proportional to the expectation value $\langle M \rangle$ of the local magnetic moment, projected onto the x-ray propagation direction; whereas XMLD is proportional to $\langle M^2 \rangle$, projected onto the x-ray polarization axis [29,34, 35]. This simplified picture neglects crystal field effects [30–32] and other changes to local anisotropy but provides a useful framework for the remainder of our analysis. A more detailed discussion on the influence of crystal field effects in the investigated systems is provided in section 1 of the supplementary material (https://stacks.iop.org/NJP/24/013030/mmedia).

Because linear dichroism is to lowest order quadratic in M, XMLD is sensitive to the spin axis of a material, rather than the spin direction, enabling the investigation of antiferromagnetic order even in the absence of a net magnetic moment.

The different sensitivities of the XMCD and XMLD effects are accounted for in their measurement geometries. XMCD is the difference in x-ray absorption that is measured with two opposite helicities of circularly polarized light, or equivalently with fixed helicity and oppositely oriented magnetization (by reversing an applied field, see figure 1(a)). For XMLD, the difference is measured by rotating either the magnetization or the linear polarization of the x-rays by 90° (e.g., figure 1(b)); the effect is maximized when these vectors are perpendicular to the x-ray propagation direction.

By combining XMLD spectroscopy with an RF excitation, we enable phase-resolved measurements of the non-equilibrium magnetization axis to study spin dynamics within a broader class of magnetic materials. Taking the relative orientation of magnetization and x-ray polarization into account, the dynamic

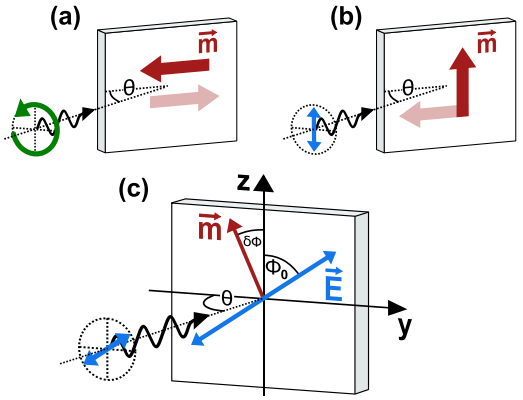

Figure 1. Standard experimental geometry for (a) static XMCD and (b) static XMLD measurements. (c) Schematic of the dynamic XMLD measurement geometry.

XMLD signal can then be written as

$$\mathrm{XMLD_{dyn.}} = I_0 \cdot \cos^2(\phi_0 + \delta\phi)\,, \tag{1}$$

where I_0 is the intensity amplitude, ϕ_0 is the angle between the equilibrium position of the magnetization vector $\vec{m}$ along a co-planar waveguide (i.e., the z-direction) and the electromagnetic polarization vector $\vec{E}$ of the incoming x-ray beam for normal incidence ($\theta = 90°$) and

$$\delta\phi \approx \delta\phi_0 \cdot \cos(\omega t) \tag{2}$$

describes the time-dependent angular displacement of the magnetization in FMR, at the RF excitation frequency ω and with a half-cone angle $\delta\phi_0$ of the precession (see figure 1(c)). Within this formalism, the magnetic precession is modeled as an oscillation of the magnetization vector in the film plane to approximate the strongly elliptical precession in the thin film regime. More details on precession shape distortion are provided in section 3 of the supplementary material.

Because the half-cone angle is typically small (<1°) at GHz frequencies, equation (1) can be expanded to 2nd order in $\delta\phi$ as

$$\begin{aligned}\mathrm{XMLD_{dyn.}} \approx\ & \frac{I_0}{2} \cdot \left(1 + \left(1 - \delta\phi_0^2\right) \cdot \cos(2\phi_0)\right) \\ & - I_0 \cdot \sin(2\phi_0) \cdot \delta\phi_0 \cdot \cos(\omega t) \\ & - I_0 \cdot \cos(2\phi_0) \cdot \frac{\delta\phi_0^2}{2} \cdot \cos(2\omega t)\,.\end{aligned} \tag{3}$$

Within this general expression, we can distinguish three distinct contributions to the dynamic XMLD response. The first term corresponds to a static XMLD signal with no time dependence and can be neglected in the ac analysis. The second term is proportional to $\cos(\omega t)$ and corresponds to the fundamental response that follows the RF excitation frequency ω, while the third term corresponds to the 2nd harmonic response (2ω). The fundamental (1ω) and the 2nd harmonic (2ω) responses exhibit different geometrical dependences and relative amplitudes. In the limit of $\phi_0 = 45°$, i.e., when the photon polarization vector is rotated 45° from the magnetization axis, the dynamic signal is dominated by the fundamental response, while higher harmonic oscillations vanish. In the cases of $\phi_0 = 0°$ and $\phi_0 = 90°$ the fundamental contribution vanishes and the dynamic response occurs only in the 2nd harmonic with opposite signs. It is noteworthy, that even small misalignments from these values can introduce additional 1ω contributions to the dynamic signal due to their relative amplitudes (1ω is larger by the factor $2/\delta\phi_0$).

To experimentally evaluate the fundamental and the 2nd harmonic responses independently, we performed dynamic XMLD experiments on the ferromagnetic metal (Py) and the ferrimagnetic insulator (NZAFO) for $\phi_0 = 0°$, $\phi_0 = 45°$, and $\phi_0 = 90°$. For each sample and measurement geometry, we performed multiple tests to verify that the dynamic signal is of magnetic origin. Notably, we confirmed that the dynamic response of the sample is zero within the statistical accuracy of the experiment under background conditions: when the photon energy is tuned to a value where no dichroism signal is present in the static spectrum, or when the experimental settings are significantly detuned from the resonance conditions. All static and dynamic x-ray absorption measurements were performed at beamline 4.0.2 of the Advanced Light Source (ALS). Details on the beamline and the experimental setup are available in

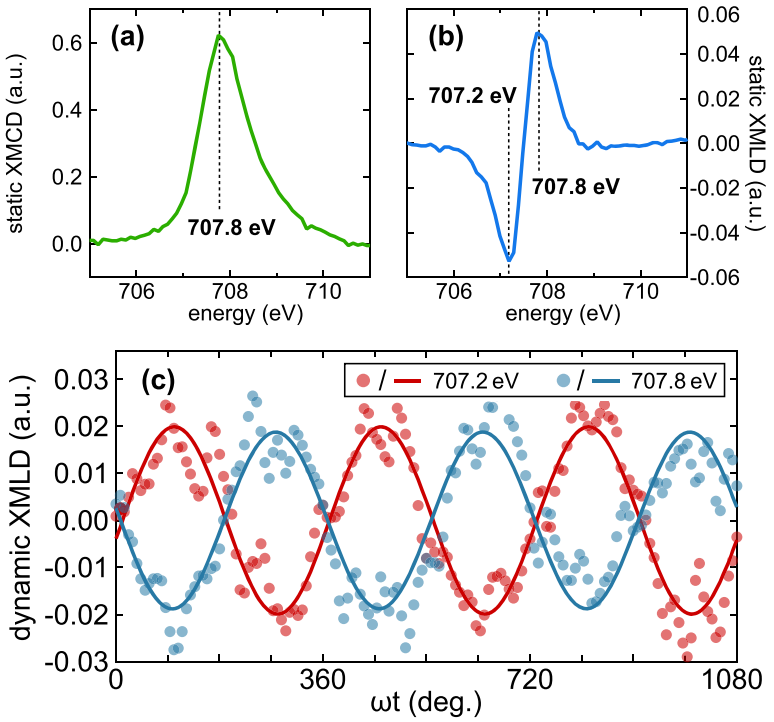

Figure 2. Static (a) XMCD and (b) XMLD spectra taken at the Fe L_3 edge of Py. (c) Dynamic XMLD phase delay scans (circles) taken at 707.2 eV and 707.8 eV with 45° x-ray polarization and corresponding sinusoidal fits (lines).

references [35–37]. The dynamic XMLD measurements are performed in a 'pump–probe' paradigm with variable delay between the periodic synchrotron x-ray pulses (500 MHz probe) and a phase-locked RF excitation (2 or 4 GHz pump). These measurements utilized a lock-in technique that enables the detection of phase dependent components of the magnetization. By incorporating phase modulation of the RF excitation we directly measure a 'difference signal' that is only finite in close proximity to the corresponding FMR field. A more comprehensive description of the small-signal detection scheme and the working principles of XFMR is provided in section 2 of the supplementary material and in reference [37].

In the first step, we carried out experiments on a 30 nm-thick Py layer. The Py film was deposited on MgO(001) substrate using molecular beam epitaxy; growth conditions were identical to those used in previous studies [7]. Static XMCD was measured in grazing incidence ($\theta = 40°$) for increased projection of the in-plane magnetic moment along the x-ray beam (cf figure 1(a)), while static and dynamic XMLD measurements were collected in normal incidence ($\theta = 90°$) (cf figures 1(b) and (c)). The static spectra at the Fe L_3 edge of Py are shown in figures 2(a) and (b), respectively. Here and throughout the rest of the paper we use the convention $\mathrm{XMLD}_{\Delta H} = I(H_{0°}, E_{\phi_0}) - I(H_{90°}, E_{\phi_0})$ to calculate the XMLD signal, where $I(H_{0°}, E_{\phi_0})$ and $I(H_{90°}, E_{\phi_0})$ correspond to the x-ray absorption signals for the magnetization vector oriented along the z-direction ($H_{0°}$) and the y-direction ($H_{90°}$) in figure 1(c), respectively, at a fixed polarization angle ϕ_0. This convention is identical to the one introduced as geometry 1 by Arenholz *et al* in reference [38]. For vertical x-ray polarization ($\phi_0 = 0°$) this is equivalent to the commonly used definition $\mathrm{XMLD} = I_{\parallel} - I_{\perp}$. However, $\mathrm{XMLD}_{\Delta H}$ proves to be more useful when interpreting dynamic data where the small FMR cone angle causes only a small projection of the precessing magnetization to change with respect to the fixed x-ray polarization (generally $\phi_0 \neq 0°$).

For the dynamic experiments, the Py film was excited into FMR using a 4 GHz RF excitation. In figure 2(c), the dynamic XMLD data from the Py sample is shown as a function of the pump–probe delay, ωt. This is typically referred to as 'phase delay scan'. The measurements were performed at the Py FMR field $\mu_0 H_{\mathrm{res}} = 22.4$ mT and repeated for two photon energies, 707.2 eV and 707.8 eV that exhibit static XMLD signals of about equal size but with opposite sign, as shown in figure 2(b). Lock-in detection was performed by 180° (125 ps) modulation of the RF phase, for maximum dynamic contrast. Figure 2(c) shows the experimental results and a 4 GHz sinusoidal fit to the data for each photon energy. The dynamic phase delay curves in figure 2(c) have nearly equal amplitude yet opposite sign, mirroring the static XMLD signal at these two energy values. The static XMCD spectrum (shown in figure 2(a)) by contrast has no sign change in this photon energy range, it is positive at 707.2 eV and 707.8 eV. This demonstrates that the

dynamic signal shown in figure 2(c) originates from the XMLD effect—not an XMCD effect—caused by the precessing magnetization.

Moreover, the correlation between the energy-dependence of the static and dynamic XMLD signals experimentally confirms the anticipated contribution at the fundamental driving frequency that dominates the dynamic response at $\phi_0 = 45°$ per equation (3). This result is a breakthrough achievement in detecting dynamic manifestations of the XMLD effect at technologically relevant, GHz frequencies. It should be noted that when using 4 GHz RF excitation, higher harmonic responses (at 8, 12, 16, …GHz) largely exceed the bandwidth of detection due to the finite pulse-width of the x-ray source ($\sim$ 70 ps FWHM). However, the 2nd harmonic response near $\phi_0 = 45°$ is expected to be negligible when compared to the fundamental signal, even for moderate misalignments of ϕ_0, due to the scaling factor $(\delta\phi_0/2)$ for that contribution.

According to equation (3) the fundamental frequency and 2nd harmonic responses are complementary in intensity with respect to the angle, ϕ_0. We therefore explored the 2nd harmonic response of dynamic XMLD using fixed x-ray polarizations, $(\phi_0 = 0°)$ or $(\phi_0 = 90°)$. These polarizations are the traditional 'vertical' or 'horizontal' designations that, respectively, are normal to or lie within the synchrotron orbit. We performed these measurements on the same Py film and also a 25 nm-thick ferrimagnetic NZAFO film. The NZAFO film was grown on (001) oriented, isostructural $MgAl_2O_4$ (MAO) substrate by pulsed laser deposition. A detailed characterization of the film properties can be found in reference [39]. While XMLD is typically small in elemental metals, it can be more sizable in transition metal oxides, which increases the signal-to-noise ratio of the dynamic experiments. Both systems yielded similar qualitative results and showed dynamic XMLD consistent with our models. In the following we concentrate on the results from the NZAFO film, due to the improved signal-to-noise ratio. The corresponding Py data is included in section 4 of the supplementary material.

Both static and dynamic spectroscopy experiments were performed with $\theta = 40°$ grazing incidence of the x-ray beam. The excitation frequency 2 GHz was selected to ensure the harmonic response was within the measurement bandwidth, which severely attenuates response frequencies above $\sim$5–6 GHz. Results from static XMCD and XMLD measurements at the Fe L_3 edge of NZAFO are presented in figures 3(a) and (b), respectively. The dichroism spectra show characteristic features typically found in ferrites with inverse spinel structure, corresponding to different valence states of the Fe cations, with magnetic moments oppositely oriented on separate tetrahedral and octahedral sublattices [38, 40–42]. The distinct differences in the lineshapes are crucial to identifying the origin of different contributions in the dynamic measurements. More details on the spectral lineshapes are provided in section 5 of the supplementary material.

We carried out phase delay scans with linearly polarized x-rays at the FMR field ($\mu_0 H_{res} = 8.0$ mT) for an excitation frequency of 2 GHz. The RF excitation was phase modulated by 90° (125 ps) to maximize the magnetic contrast in this geometry.

Results from a phase delay scan taken at $E = 708.8$ eV with vertical polarization $(\phi_0 = 0°)$ are shown in figure 3(c). The observed signal shows a pronounced oscillation with both fundamental and 2nd harmonic contributions. According to equation (3), we expect the dynamic XMLD to be contained entirely in the 2nd harmonic response (4 GHz) for $\phi_0 = 0°$, while no fundamental 2 GHz effect should be present in this geometry. The relative amplitudes for the different contributions can be determined by fitting the data with a 2nd order Fourier series. In order to identify the origin of the unexpected fundamental contribution, we measured the dynamic response as a function of x-ray energy across the L_3 absorption edge with vertical and horizontal x-ray polarizations. By analyzing the data for its 1ω (2 GHz) and 2ω (4 GHz) components we can directly extract the amplitude of the dynamic response at each photon energy and reproduce the full L_3 spectrum. The results are shown in figure 4.

Figure 4(a) displays the Fourier series contributions from dynamic measurements with vertically polarized x-rays. The 2nd harmonic component reproduces all the characteristic features of the static XMLD spectrum. This is clear evidence for dynamic XMLD present in the 2ω response. In contrast, the fundamental component closely resembles the lineshape of the static XMCD spectrum. Circular dichroism should be entirely absent when measuring with linear x-ray polarization and here indicates a mixed polarization setting of the x-ray source. By analyzing the degree of x-ray polarization, we find a circular component of $\sim$6% in the polarized x-rays at the time of these measurements. By separating the 1ω and 2ω contributions in this experimental geometry, one can eliminate the effects of incomplete polarization of the source to isolate the pure dynamic XMLD response.

The results from phase delay scans with horizontally polarized $(\phi_0 = 90°)$ x-rays are shown in figure 4(b). In this case with source polarization settings optimized [degree of linear polarization 100% (<1% uncertainty)], both the fundamental and 2nd harmonic components exhibit a lineshape similar to the static XMLD. While we expect a dynamic XMLD signal in the 2nd harmonic response, the 1ω component likely arises from a small misalignment between the sample magnetization and the photon

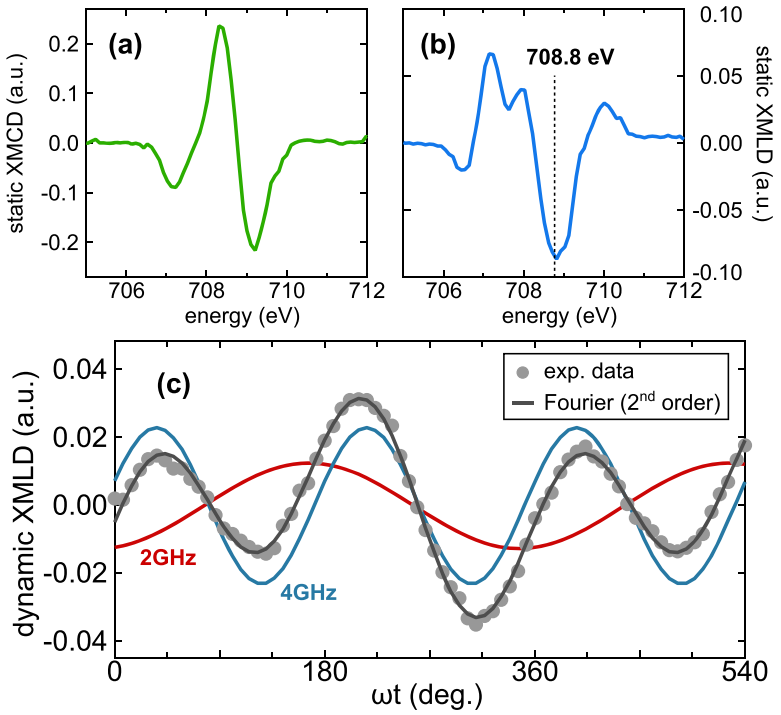

Figure 3. Static (a) XMCD and (b) XMLD spectra taken at the Fe L_3 edge of NZAFO. (c) Dynamic XMLD phase delay scan taken with vertically polarized ($\phi_0 = 0°$) x-rays at $E = 708.8$ eV. The experimental data is fitted with a Fourier extension to 2nd order and evaluated for its 1st (2 GHz, red) and 2nd harmonic (4 GHz, blue) components.

polarization vector. Due to the different relative amplitudes of the 1ω and 2ω terms in equation (3), even a small misalignment of the sample during mounting on the order of 0.1° from the nominal $\phi_0 = 90°$, can induce a sizable 1ω contribution to the dynamic signal.

As shown here we can obtain a robust dynamic XMLD signal by isolating the 2nd harmonic response via Fourier component analysis, as represented by the blue trace in figures 4(a) and (b). Note that in figure 4(b), both the dynamic XMLD and the static XMLD spectra were captured with horizontally polarized ($\phi_0 = 90°$) x-rays. The reversed sign of the static XMLD spectrum in figure 4(b) with respect to that shown in figure 3(b) is a direct consequence of the $\text{XMLD}_{\Delta H}$ convention. The observed agreement between the dynamic and static XMLD (at fixed x-ray polarization) plus the sign reversal that accompanies rotation of the polarization vector by 90° further confirms the validity of our dynamic XMLD model. Differences in relative amplitude for the two linear polarizations can be attributed to an elliptical distortion of the precession due to magnetic anisotropy in the NZAFO thin film. This is confirmed by additional simulations using a geometrical model accounting for the precession shape and the different measurement geometries (see section 6 of the supplementary material).

In conclusion, we have presented the first theoretical and experimental realization of dynamic XMLD in a ferro- and a ferrimagnetic reference system. By using linearly polarized x-rays, we were able to observe a pronounced XMLD signal from the RF magnetic resonance of magnetic moments in ferromagnetic Py and ferrimagnetic NZAFO. Our calculated and experimental observations demonstrate the importance of experimental geometry in highlighting different contributions to the dynamic signal. The dynamic XMLD response occurs primarily at the same frequency as the driving RF excitation when the angle between static magnetization and x-ray polarization is near $\phi_0 = 45°$. This effect is well suited for in-plane magnetic anisotropy studies conducted in normal incidence geometry. For studies that require complementary geometries (e.g., vertical or horizontal polarization, $\phi_0 = 0°$ or $\phi_0 = 90°$), the dynamic signal can be extracted from the 2ω response. This works also for grazing incidence measurements that are sensitive to in-vs out-of-plane magnetic anisotropy. An added benefit of the Fourier component analysis, is that the 2ω response substantially reduces sensitivity to experimental misalignments and the degree of polarization purity in the x-ray source.

Our experiments establish dynamic XMLD as a functional probe of GHz magnetization dynamics in FMs and also in materials with antiparallel alignment of magnetic moments. The combination of fundamental and 2nd harmonic components within the complementary angle space expands the useful range of experimental geometries, enabling practical measurements of dynamic XMLD that can be tailored individually to the system under study. By utilizing the sensitivity of XMLD to the spin axis rather than the

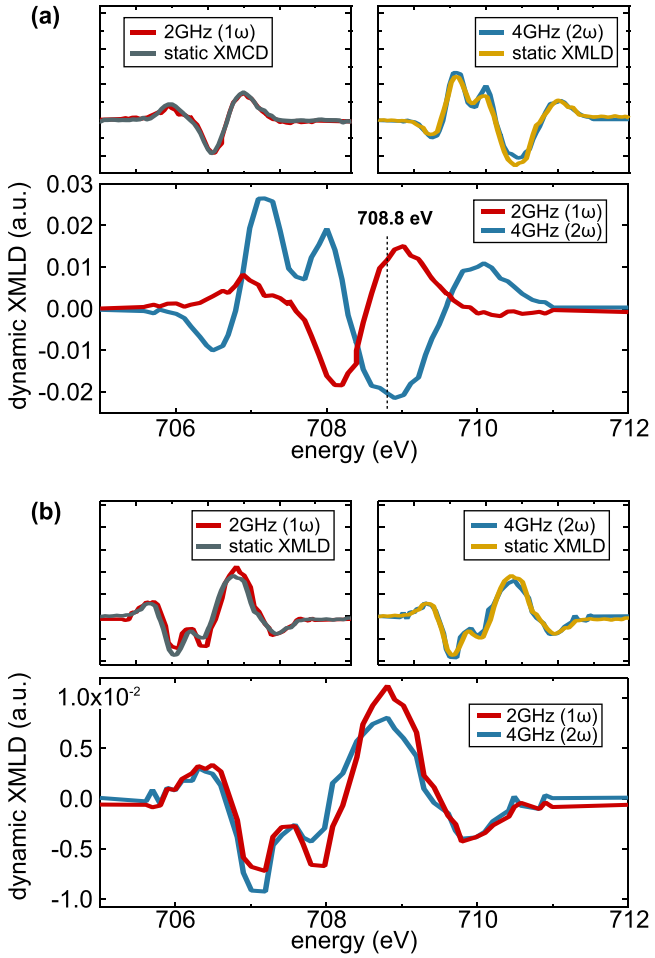

Figure 4. Dynamic signal as a function of energy taken at the Fe L_3 edge of NZAFO with (a) vertically ($\phi_0 = 0°$) and (b) horizontally ($\phi_0 = 90°$) polarized x-rays. For vertical polarization the 4 GHz component corresponds to the contribution from dynamic XMLD while the 2 GHz components can be attributed to a spurious dynamic XMCD signal. For horizontal x-ray polarization, both components show a pronounced XMLD lineshape.

spin direction, one can expand the reach of XFMR to enable studies of GHz driven magnetization dynamics in antiferromagnetically ordered systems.

Furthermore, we believe that our demonstration of time-resolved dynamic XMLD lays the foundation for future sub-THz and THz studies of antiferromagnetically ordered materials, which could be achieved by combining dynamic XMLD with the time-resolution of XFEL facilities or gyrotron sources [43, 44, 46]. Such studies hold considerable promise for further explorations of antiferromagnetic spintronics.

Acknowledgments

This research used resources of the Advanced Light Source, a DOE Office of Science User Facility under Contract No. DE-AC02-05CH11231. SE and YS were supported by a Vannevar Bush Faculty Fellowship sponsored by the Basic Research Office of the Assistant Secretary of Defense for Research and Engineering and funded by Office of Naval Research Grant No. N00014-15-1-0045. SE was also supported in part by NSF Grant No. DMR-2003914. YS was also supported by US Department of Energy, Director, Office of Science, Office of Basic Energy Sciences, Division of Materials Sciences and Engineering under Contract No. DESC0008505. ZQ acknowledges financial support by US Department of Energy, Office of Science, Office of Basic Energy Sciences, Materials Sciences and Engineering Division under Contract No. DE-AC02-05CH11231 (van der Waals heterostructures program, KCWF16). This material is based upon work supported by Dr. Ken Goretta (Program Manager) at the Air Force Office of Scientific Research under Award No. FA9550-15RXCOR198.

Data availability statement

All data that support the findings of this study are included within the article (and any supplementary files).

ORCID iDs

C Klewe https://orcid.org/0000-0002-5816-5647
P Shafer https://orcid.org/0000-0001-9363-2557

References

[1] Fukami S, Zhang C, DuttaGupta S, Kurenkov A and Ohno H 2016 *Nat. Mater.* **15** 535–41
[2] Oh Y-W *et al* 2016 *Nat. Nanotechnol.* **11** 878–84
[3] Hahn C, de Loubens G, Naletov V V, Ben Youssef J, Klein O and Viret M 2014 *Europhys. Lett.* **108** 57005
[4] Wang H, Du C, Hammel P C and Yang F 2014 *Phys. Rev. Lett.* **113** 097202
[5] Qiu Z *et al* 2016 *Nat. Commun.* **7** 12670
[6] Lin W, Chen K, Zhang S and Chien C L 2016 *Phys. Rev. Lett.* **116** 186601
[7] Li Q *et al* 2019 *Nat. Commun.* **10** 5265
[8] Dabrowski M *et al* 2020 *Phys. Rev. Lett.* **124** 217201
[9] Li J *et al* 2020 *Nature* **578** 70
[10] Vaidya P, Morley S A, van Tol J, Liu Y, Cheng R, Brataas A, Lederman D and del Barco E 2020 *Science* **368** 160–5
[11] Schütz G, Wagner W, Wilhelm W, Kienle P, Zeller R, Frahm R and Materlik G 1987 *Phys. Rev. Lett.* **58** 737
[12] Chen C T, Sette F, Ma Y and Modesti S 1990 *Phys. Rev.* B **42** 7262
[13] Stöhr J 1995 *J. Electron Spectrosc. Relat. Phenom.* **75** 253
[14] Bailey W E, Cheng L, Keavney D J, Kao C-C, Vescovo E and Arena D A 2004 *Phys. Rev.* B **70** 172403
[15] Boero G, Rusponi S, Bencok P, Popovic R S, Brune H and Gambardella P 2005 *Appl. Phys. Lett.* **87** 152503
[16] Goulon J, Rogalev A, Wilhelm F, Jaouen N, Goulon-Ginet C, Goujon G, Ben Youssef J and Indenbom M V 2005 *JETP Lett.* **82** 696–701
[17] Arena D A, Vescovo E, Kao C-C, Guan Y and Bailey W E 2006 *Phys. Rev.* B **74** 064409
[18] Guan Y, Bailey W E, Vescovo E, Kao C-C and Arena D A 2007 *J. Magn. Magn. Mater.* **312** 374
[19] Martin T, Woltersdorf G, Stamm C, Dürr H A, Mattheis R, Back C H and Bayreuther G 2009 *J. Appl. Phys.* **105** 07D310
[20] Marcham M K *et al* 2011 *J. Appl. Phys.* **109** 07D353
[21] Stenning G B G *et al* 2015 *New J. Phys.* **17** 013019
[22] Warnicke P *et al* 2015 *Phys. Rev.* B **92** 104402
[23] Figueroa A I, Baker A A, Collins-McIntyre L J, Hesjedal T and van der Laan G 2016 *J. Magn. Magn. Mater.* **400** 178
[24] Baker A A, Figueroa A I, Love C J, Cavill S A, Hesjedal T and van der Laan G 2016 *Phys. Rev. Lett.* **116** 047201
[25] Li J *et al* 2016 *Phys. Rev. Lett.* **117** 076602
[26] Durrant C J *et al* 2017 *Phys. Rev.* B **96** 144421
[27] van der Laan G, Thole B T, Sawatzky G A, Goedkoop J B, Fuggle J C, Esteva J-M, Karnatak R, Remeika J P and Dabkowska H A 1986 *Phys. Rev.* B **34** 6529
[28] Alders D, Tjeng L H, Voogt F C, Hibma T, Sawatzky G A, Chen C T, Vogel J, Sacchi M and Iacobucci S 1998 *Phys. Rev.* B **57** 11623
[29] Kuiper P, Searle B G, Rudolf P, Tjeng L H and Chen C T 1993 *Phys. Rev. Lett.* **70** 1549
[30] Arenholz E, van der Laan G, Chopdekar R V and Suzuki Y 2007 *Phys. Rev. Lett.* **98** 197201
[31] van der Laan G, Arenholz E, Chopdekar R V and Suzuki Y 2008 *Phys. Rev.* B **77** 064407
[32] van der Laan G, Arenholz E, Schmehl A and Schlom D G 2008 *Phys. Rev. Lett.* **100** 067403
[33] Boero G, Rusponi S, Bencok P, Meckenstock R, Thiele J-U, Nolting F and Gambardella P 2009 *Phys. Rev.* B **79** 224425
[34] van der Laan G, Thole B T, Sawatzky G A, Goedkoop J B, Fuggle J C, Esteva J-M, Karnatak R, Remeika J P and Dabkowska H A 1986 *Phys. Rev.* B **34** 6519
[35] Advanced Light Source 2021 als.lbl.gov/beamlines/4-0-2/
[36] Young A T, Arenholz E, Feng J, Padmore H, Marks S, Schlueter R, Hoyer E, Kelez N and Steier C 2002 *Surf. Rev. Lett.* **09** 549–54
[37] Klewe C *et al* 2020 *Synchrotron Radiat. News* **33** 12–9
[38] Arenholz E, van der Laan G, Chopdekar R V and Suzuki Y 2006 *Phys. Rev.* B **74** 094407
[39] Emori S *et al* 2017 *Adv. Mater.* **29** 1701130
[40] Pattrick R A D, van der Laan G, Henderson C M B, Kuiper P, Dudzik E and Vaughan D J 2002 *Eur. J. Mineral.* **14** 1095
[41] Klewe C, Meinert M, Boehnke A, Kuepper K, Arenholz E, Gupta A, Schmalhorst J-M, Kuschel T and Reiss G 2014 *J. Appl. Phys.* **115** 123903
[42] Hoppe M, Döring S, Gorgoi M, Cramm S and Müller M 2015 *Phys. Rev.* B **91** 054418
[43] Rogalev A, Goulon J, Goujon G, Wilhelm F, Ogawa I and Idehara T 2012 *J. Infrared Millim. Terahertz Waves* **33** 777–93
[44] Shalaby M, Vidal F, Peccianti M, Morandotti R, Enderli F, Feurer T and Patterson B D 2013 *Phys. Rev.* B **88** 140301(R)
[45] Thole B T, van der Laan G and Sawatzky G A 1985 *Phys. Rev. Lett.* **55** 2086
[46] Němec P, Fiebig M, Kampfrath T and Kimel A V 2018 *Nat. Phys.* **14** 229–41